Formulation of two monofunctionnal catalysts for CH4 upgrading

Stanislav Konnov, Izabel Medeiros-Costa, Hugo Cruchade, Florent Dubray, Maxime Debost, Jean-Pierre Gilson, Valentin Valtchev, Jean-Pierre Dath, Nikolai Nesterenko, Svetlana Mintova

Formulation of two monofunctionnal catalysts for CH_4 upgrading

Stanislav V. Konnov[a], *Izabel C. Medeiros-Costa*[a], *Hugo Cruchade*[a], *Florent Dubray*[a], *Maxime Debost*[a,b], *Jean-Pierre Gilson*[a], *Valentin Valtchev*[a], *Jean-Pierre Dath*[c], *Nikolai Nesterenko*[c], *Svetlana Mintova*[a,*]

[a]Normandie Université, ENSICAEN, UNICAEN, CNRS, Laboratoire Catalyse et Spectrochimie (LCS), 14050 Caen, France.

[b]Normandie Université, ENSICAEN, UNICAEN, CNRS, Laboratoire de Cristallographie et Science des Matériaux (CRISMAT), 14050 Caen, France.

[c]Total Research and Technology, Feluy, B-7181 Seneffe, Belgium.

*Corresponding author svetlana.mintova@ensicaen.fr

ABSTRACT

Natural gas will play a significant role in the transition from fossil to green(er) energy production. Its major component, methane (CH_4) is an attractive resource to co-generate hydrogen (H_2) and added value chemicals (important building blocks such as olefins and aromatics) for petrochemistry. We highlight the advantage of using a novel dual catalyst system containing a monofunctional Al-free metallic single site catalyst referred as S-Mo (Si/Al ~ ∞) where Mo is atomically dispersed in the zeolitic framework and a monofunctional acidic H-ZSM-5 catalyst referred as S-Al (Si/Al = 128) to achieve superior yields of high value products. Under severe reaction (850 ºC) and regeneration (700 ºC) conditions, the Mo-S catalyst is stable and does not suffer from irreversible structural damage by losing its Mo atomic dispersion, and deactivation by coke deposition, thus ensuring steady catalytic performances in multi-cycle catalytic tests. Conversely, the current bifunctional catalysts prepared by Mo impregnation on an acidic catalyst suffer from irreversible damage during coke combustion due to the formation of $Al_2(MoO_4)_3$ or $AlMoO_6$ Anderson entities. This new approach opens novel and promising pathways to develop methane upgrading processes based on the physical separation and operation of a non-deactivating metallic catalyst and a regenerable acidic catalyst.

KEYWORDS: dual catalysts, Mo single-site zeolite, ZSM-5 zeolite, high stability, methane conversion, hydrocarbons production, regenerability.

1. Introduction

Two main drivers power a continuous increase in energy and chemicals demand: expanding demographics and the increasing purchasing power of a growing middle class [1]. Many challenges are associated, such as the need to decrease steadily the overall carbon footprint of human activity. Natural gas is poised to play a significant role in the long transition from fossil to green energy production. Methane, its major constituent, can be transformed in hydrogen and its carbon, combined with some hydrogen, removed as valuable chemicals such as lower olefins and aromatics with a minimum release of capturable greenhouse-gas emissions (*e.g.* CO_2).

At present, the dominant commercial processes to valorize methane involve an indirect technology where methane reacts with water (steam reforming) or with oxygen (partial oxidation) to form synthesis gas (CO and H_2 of variable composition), a dual platform to produce fuels and chemicals [2,3]. The drawbacks of such processes are high energy demand and carbon footprint, moderate carbon efficiency, high capital intensity, and high purity requirements for the feedstocks [2,4]. A direct conversion of methane into hydrogen, liquid chemicals and fuels is a more appealing and promising alternative.

The oxidative coupling of methane (OCM) to C_2H_6 and C_2H_4 has been extensively investigated for decades. However, OCM has two main drawbacks preventing its commercialization: (i) the yield of C_2 chemicals typically does not exceed 25%, and (ii) the presence of oxygen promotes to formation of CO_2 [3,5–7]. Nonoxidative direct methane conversion processes include pyrolysis producing pure hydrogen and solid carbon without direct CO_2 emissions [8], non-oxidative coupling producing C_2 hydrocarbons [9,10] and conversion to hydrogen and higher hydrocarbons (a mixture of aromatics and/or C_2 products) [4,11]. The latter has attracted significant attention from both academia and industry.

Methane conversion to hydrogen and aromatics, often referred to as MDA (Methane DehydroAromatization) is highly endothermic and therefore requires high temperatures (above 650 °C) to produce acceptable yields of the desired hydrocarbons [4,11–13]. One of the major challenges hindering its commercialization is a fast and irreversible deactivation of its bi-functional catalyst, typically a Mo-impregnated H-ZSM-5 or H-MCM-22 zeolite, due to a

reaction between the zeolitic Al and the Mo during regeneration leading to the formation of a stable $AlMoO_6$ phase [14].

Despite decades of intensive investigation of conventional Mo-containing ZSM-5 catalyst (Mo/ZSM-5), commercialization is still far from being possible [15]. Recently Guo *et al.* [9], Yao *et al.* [16], Xie *et al.* [17], proposed new catalysts for methane conversion to hydrogen and hydrocarbons displaying high stability, high carbon efficiency due to negligible coke formation and improved regenerability. Contrary to the current bifunctional Mo-impregnated ZSM-5 catalysts, their features are (i) single-site metal catalysts, (ii) low or zero activity at 700 °C, and (iii) higher C_2 yields.

Recently we reported a novel Mo-containing nanosized ZSM-5 (Si/Al=110) zeolite ([Mo]ZSM-5), with atomically dispersed framework-molybdenum homogenously distributed through the zeolite crystals [14]. It showed superior thermal (up to 1000 °C), hydrothermal (steaming) stability in the conversion of methane to hydrogen and higher hydrocarbons. Despite harsh operating conditions, the structural integrity of the zeolite (atomic dispersion of the Mo and absence of silanol defects) was maintained. Such a [Mo]ZSM-5 zeolite catalyst (0.5 m% Mo) shows exceptional stability in the conversion of CH_4 after three cycles of reaction (850 °C)/regeneration (700 °C), in stark contrast to a reference catalyst obtained by the currently used metal impregnation. Moreover, the [Mo]ZSM-5 catalyst produces an almost constant yield of hydrogen and higher hydrocarbons throughout catalytic tests [14]. Its main drawback is a partial dealumination of the zeolite (ZSM-5) during reaction-regeneration cycles, decreasing the number of Brønsted acid sites (BAS) and aromatics yield.

Controlling the distance between active sites in some of the existing bifunctional MDA catalysts to improve their performances has already been studied. Zeng *et al.* investigated various Mo/H-MCM-22 catalysts obtained by hydrothermal synthesis, wet impregnation, mechanical milling, physical mixing and dual catalytic beds to control the distance between the metal and acid sites (from $9.0 \cdot 10^{-3}$ to $1.5 \cdot 10^{4}$ µm) [18]. A Mo/HMCM-22 obtained by mechanical milling where the distance between the metal and acid sites was $1 \cdot 10^{-1}$ µm displayed the best catalytic performances (lower coke deposition and higher benzene selectivity). Others highlighted a synergistic effect on catalysts made of physical mixtures of (i) Mo deposited on a support and (ii) aluminum containing zeolites [2,19,20]. This suggests that the proximity of acid and metal functions could be a key to maintain steady catalytic performance.

Kosinov *et al.* investigated physical mixtures of supported Mo (on ZSM-5, SiO_2, γ-Al_2O_3, and activated carbon) and ZSM-5 [2]. The synergy observed was due to migration of molybdenum oxides from their support to the zeolite. They concluded that the main function of the ZSM-5 zeolite is to provide (i) a shape-selective environment for the conversion of methane to benzene and (ii) BAS promoting the dispersion of the Mo-oxide precursor and the active Mo-carbide phase inside the pores of the zeolite.

The dual bed approach is moderately considered in academia [21–23] and industry [24]. Recently, a process for direct methane conversion based on a physical separation of Mo and acidic catalyst for effective regeneration of individual components was reported [25]. This allows (i) methane activation to C_2 hydrocarbons and their subsequent oligomerization to take place under optimal conditions by adjusting the composition of the catalyst to tune the C_2/aromatics ratio, and (ii) effective regeneration of the individual components.

Our work is derived from such an observation and reports a dual zeolite catalyst system containing a monofunctional Al-free "single site" hereinafter referred to as S-Mo and a monofunctional acidic H-ZSM-5 hereinafter referred to as S-Al used in two configurations:

- a physical mixture (referred to as D-M) of the S-Mo and S-Al catalysts
- a layered bed (referred to as D-L) with the S-Mo catalyst on top and the S-Al at the bottom

The layered bed option allows methane activation and transformation to C_2 hydrocarbons in the top section followed by oligomerization in the bottom section under separately optimized conditions (temperature).

2. Experimental

2.1. Synthesis of MFI-type zeolites: ZSM-5 and Silicalite-1

These two zeolites were synthesized using the following reagents: tetraethyl orthosilicate (TEOS, 98%, Aldrich), tetra-*n*-propylammonium hydroxide (TPAOH, 20 wt.% in aqueous solution, Alfa Aesar), double-distilled water and aluminum nitrate ($Al(NO_3)_3.9H_2O$, 97%, Prolabo).

The chemical compositions of the precursor suspensions were:

- ZSM-5: 1 SiO_2: 0.357 TPAOH: 0.004 Al_2O_3: 16.189 H_2O
- Silicalite-1: 1 SiO_2: 0.4 TPAOH: 40 H_2O

TPAOH and water were first mixed for about 30 min under magnetic stirring. For ZSM-5, the Al source was added in the initial mixture together with TPAOH and water. For both syntheses the TEOS was added dropwise to the initial mixtures at the end after 30 min stirring; precursor suspensions were aged for 18 h at room temperature on an orbital shaker. For ZSM-5 the aged precursor suspensions were transferred into a 20 mL teflon-lined autoclave, and subjected to hydrothermal treatment at 180 °C for 72 h under autogenous pressure. In the case of silicalite-1, the aged suspensions in propylene bottles were directly placed in the oven at 90 °C for 48 h under autogenous pressure. The harvested solids were washed repeatedly with double-distilled water and high-speed centrifugation, until the pH of the supernatant was below 8. The samples were dried at 80 °C and calcined at 550 °C for 5 h. The Si/Al ratio of the ZSM-5 was 128 and its particle size about 200 nm. The size of the Silicalite-1 crystals was about 100 nm.

Mo was incorporated in the silicalite-1 framework as follows: 1.2 g of the parent calcined silicalite-1 (vide supra) were mixed in a 125 mL polypropylene bottle with a solution containing 0.8 g of sodium molybdate ($Na_2MoO_4.4H_2O$, 98 percent, Alfa Aesar) solubilized in 25 mL of double-distilled water. The mixture was heated under autogenous pressure for 7 days at 90 °C and referred to as **S-Mo**. The crystals were washed and centrifugated (20.000 rpm) until the pH of supernatant was 8.5, then dried at 80 °C overnight and further calcined under air for 5 h at 550 °C. S-Mo was ion-exchanged with a solution of NH_4Cl (0.2 M) in two successive cycles under magnetic stirring of 1 h each, dried overnight and calcined at 550 °C for 5 h. The Mo loading determined by EDS was 0.5 wt. %. The as synthesized ZSM-5 was ion-exchanged with a solution of NH_4Cl (0.2 M) in two successive cycles under magnetic stirring of 1 h each and labelled **S-Al.**

Both S-Mo and S-Al were used to prepare dual catalysts either as a physical mixture (**D-M**) or a layered configuration (**D-L**); all samples are summarized in Table 1.

Table 1. Catalysts used in non-oxidative high temperature CH_4 conversion.

Catalyst	Description
S-Mo (Mo-Silicalite-1)	0.5 % Mo in Silicalite-1 framework prepared by post synthesis hydrothermal treatment
S-Al (H-ZSM-5)	H-ZSM-5 with Si/Al=128
D-M (Dual mixed catalyst - M)	Mixture of S-Mo and S-Al catalysts
D-L (Dual layered catalyst - L)	Layered catalyst consisting of S-Mo (top) and S-Al (bottom)
S-Mo-L-AR **S-Mo-L-AR-R**	S-Mo after reaction from the dual layered catalyst (D-L) S-Mo after reaction and regeneration from the dual layered catalyst (D-L)
S-Al-L-AR **S-Al-L-AR-R**	S-Al after reaction from the dual layered catalyst (D-L) S-Al after reaction and regeneration from dual layered catalyst (D-L)
D-M-AR	Dual mixed catalyst (mixture of S-Mo and S-Al catalysts) after reaction

2.2. Characterization

X-Ray diffraction patterns of zeolites were recorded on a PANanalytical X'Pert Pro diffractometer equipped with a Johansson monochromator set up for Cu, with Kα1 radiation λ = 1.540598 Å. The patterns were acquired with steps of 0.0167 °. Unit cell parameters were calculated using the Le Bail profile refinements on the JANA2006 software [26].

Crystallinity and local silicon and aluminum environments were characterized by ^{29}Si and ^{27}Al solid-state MAS NMR, respectively. ^{29}Si and ^{27}Al NMR spectra were acquired on a Bruker Avance III-HD 500 MHz (11.7 T) spectrometer operating at 99.3 MHz and 130.3 MHz for ^{29}Si and ^{27}Al, respectively. A 4 mm zirconia rotor was used for measurements performed at a 14 KHz spinning. Single pulse excitations were used, with a flip angle of 30° and 90° corresponding to radio frequency fields of 38 KHz and 188 KHz for ^{29}Si and ^{27}Al, respectively. ^{29}Si NMR spectra (2048 scans) were measured with a D1 of 20s. ^{27}Al NMR spectra (4096 scans) were acquired using a D1 of 1 s. Tetramethylsilane (TMS) and aluminium nitrate ($Al(NO_3)_3$) were used as references for the ^{29}Si and ^{27}Al NMR chemical shifts, respectively.

The crystal size, morphology and crystallinity of all catalysts were determined by high-resolution transmission electron microscopy (HR-TEM) using a FEI Tecnaï G2 (LaB6-300 kV).

The combustion of the coke on all spent catalysts was monitored by thermogravimetric analysis (TGA) using a SETSYS (SETERAM, Caluire, France) thermobalance. Samples were heated in uncovered alumina crucibles at a rate of 10 °C/min from room temperature to 1000 °C under a 40 ml/min flow of dry air.

2.3 Catalytic performances in CH_4 conversion

All catalysts were pelletized, crushed, sieved and the 200–400 µm fraction retained for testing in a quartz downflow tubular reactor (367 mm long and 6.0 mm of internal diameter). In the layered bed configuration (D-L), 0.2 g of each catalyst (top: S-Mo, bottom: S-Al) diluted (1/1) with silicon carbide pellets of 300 µm catalyst were sandwiched between a quartz wool layer. In the mixed configuration (D-M), S-Mo (0.2 g, 200–400 µm) and S-Al (0.2 g, 200–400 µm) were directly mixed together with silicon carbide as in D-L.

The conditions for the catalytic tests were: T = 850 °C, P = 1 bar, WHSV = 1.2 h^{-1}. Before reaction, all catalysts were activated from room to the reaction temperature (ramp rate of 10 °C/min) under a flow of CH_4/N_2 (80/20 vol. %). The products were analyzed online with an Interscience Compact GC chromatograph fitted with three channels. The GC three-channel configuration included two TCD, and one FID detectors on dedicated columns (Molsieve 5A, Rt-QBond, Rtx-1) to analyze light gases (H_2, N_2, CO, CO_2), light hydrocarbons (CH_4, C_2H_4, C_2H_6) and aromatic hydrocarbons (benzene, toluene, xylenes, ethylbenzene, naphthalene). Nitrogen was used as an internal standard.

The methane conversion (X_{CH_4}) was calculated according to the following equation:

$$X_{CH_4}(\%) = \frac{\left(\frac{A_{CH_4}}{A_{N_2}}\right)^{In} - \left(\frac{A_{CH_4}}{A_{N_2}}\right)^{Out}}{\left(\frac{A_{CH_4}}{A_{N_2}}\right)^{In}} \times 100$$

With A_{CH_4} and A_{N_2} the gas chromatography areas of methane and nitrogen respectively in the gas mixture, at the inlet (exponent In) and outlet (exponent Out) of the reactor.

The yields of hydrocarbon products ($Y_{C_xH_y}$) expressed in % were calculated according to:

$$Y_{C_xH_y}(\%) = \frac{x \times F_{C_xH_y}^{Out}}{F_{CH_4}^{In}} \times 100$$

With x the number of carbon atoms in the molecule, $F_{C_xH_y}^{Out}$ the molar flow rate of the compound C_xH_y at the outlet of the reactor and $F_{CH_4}^{In}$ the molar flow rate of methane at the reactor inlet.

The overall yields of hydrocarbon products ($Y_{C_xH_y}$) on a time on stream window (*i.e.* between t_1 and t_2), expressed in mg $g_{Cat.}^{-1}$, were calculated according to:

$$Y_{C_xH_y}(\text{mg } g_{Cat.}^{-1}) = \frac{1}{m_{Cat.}} \times \int_{t_1}^{t_2} \left(F'^{Out}_{C_xH_y}\right) dt$$

With $F'^{Out}_{C_xH_y}$ the mass flow rate of compound C_xH_y at the reactor outlet and $m_{Cat.}$ the mass of catalyst.

The carbon balance was closed to determine the amount of coke formation. The value of the total quantity of produced coke based on mass balance was in agreement with TGA measurements.

Reaction-regeneration cycles of the catalysts were performed as follows: after each catalytic test, the reactor was cooled to room temperature under a dry nitrogen flow (10 mL/min) followed by regeneration under a dry air flow (15 mL/min) from room temperature to 700 °C (2 °C/min, isotherm for 3 h). In the case of the layered catalyst, D-L, the deactivated bottom layer (S-Al) was replaced by a fresh one for every subsequent catalytic cycle.

3. Results and discussion.

The S-Mo catalyst contains 0.5 wt. % Mo according to EDS-TEM and ICP analyses [14]. Mo insertion in the MFI framework is confirmed by XRD (Figure 1A), in particular a transition to monoclinic symmetry and an increased unit cell volume as reported earlier (Table 2) [27]. Further evidence of framework Mo incorporation is provided by ^{29}Si NMR spectroscopy: highly resolved Q^4 peaks, typical of defect-free structures (Figure 1B). We reported this earlier and attributed it to the healing of silanol defects during the insertion of Mo atoms in the zeolitic framework [14,28].

The high crystallinity of S-Al (H-ZSM-5) is confirmed by X-ray diffraction (Figure 1A) while ^{29}Si NMR indicates that it contains more defects than S-Mo as the resolution of its Q^4 peak is lower. Moreover, the presence of a Q^3 signal indicates the presence of both bridged hydroxyls and silanols.

3.1 Catalytic performance of single (S-Mo, S-Al) and dual (D-M, D-L) catalysts.

The catalytic performances are evaluated in the conversion of CH_4 to hydrogen and hydrocarbons (850 °C, atmospheric pressure, WHSV = 1.2 h^{-1}). S-Mo (metallic) is used either as a single catalyst or combined with S-Al (acidic) in two different configurations, Figure 2. D-M is a physical mixture of S-Mo and S-Al catalysts in a single bed (Table 1) while D-L is a layered bed of S-Mo (top) and S-Al (bottom).

Their performances are outlined in Figure 3A (conversion as a function of time on stream) and Figure 3B (products yields). Methane conversion and products yield are calculated from the first 250 min on stream (aromatics: benzene, toluene, xylenes, ethylbenzene and naphthalene, aliphatics: ethylene, ethane, traces of C_3-C_5 hydrocarbons (less than 0.3% of selectivity) and coke.

Table 2. Unit cell parameters (Le Bail refinement of the XRD patterns) of catalysts before (S-Al and S-Mo) and after methane conversion and regeneration at 700 °C (S-Al-L-AR-R and S-Mo-L-AR-R).

Catalyst	Symmetry	*a* (Å)	*b* (Å)	*c* (Å)	B (°)	V (Å^3)	wRp
S-Al	*pnma*	19.906	20.099	13.396	90	5359.8	6.2
S-Al-L-AR-R	*pnma*	19.889	20.069	13.387	90	5343.4	6.6
S-Mo	*p21/n*	19.915	20.130	13.390	90.589	5367.6	3.5

S-Mo-L-AR-R	*p21/n*	19.920	20.137	13.398	90.592	5374.1	3.6

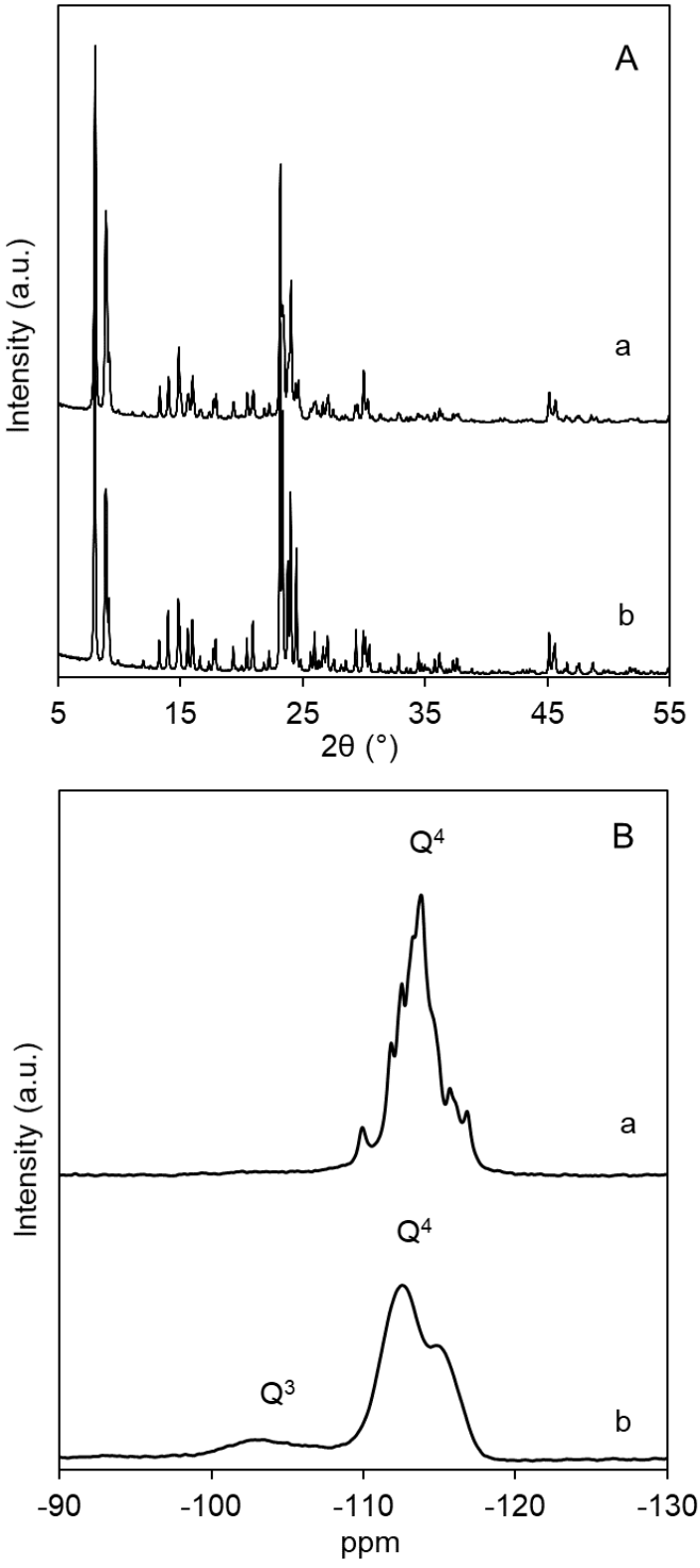

Figure 1. (A) X-ray diffraction patterns and (B) ^{29}Si MAS NMR spectra of (a) S-Mo and (b) S-Al catalysts. ^{29}Si MAS NMR spectra are normalized to identical number of scans and mass.

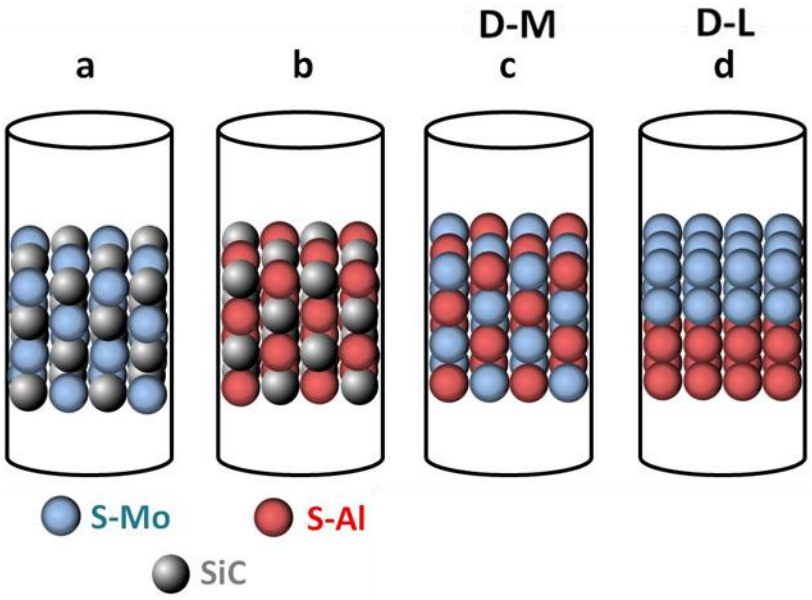

Figure 2. Schematic representation of the catalysts: (a) S-Mo diluted with with SiC, (b) S-Al (diluted with SiC, (c) D-M (physical mixture of S-Mo and S-Al), (d) D-L with S-Al (bottom) and S-Mo (top).

S-Mo alone displays a very low conversion (< 1%) to aliphatic hydrocarbons and coke. The conversion increases significantly when S-Al is added (D-M and D-L) to form a dual catalyst system; D-L converting more than D-M but mostly to coke. In DM, S-Al in the upper layer cannot effectively produce aromatics, since C_2 production by S-Mo is limited. On the layered D-L catalysts, S-Mo is on the top layer and produces more C_2 intermediates further converted to aromatics, hydrogen and coke on bottom layer with S-Al.

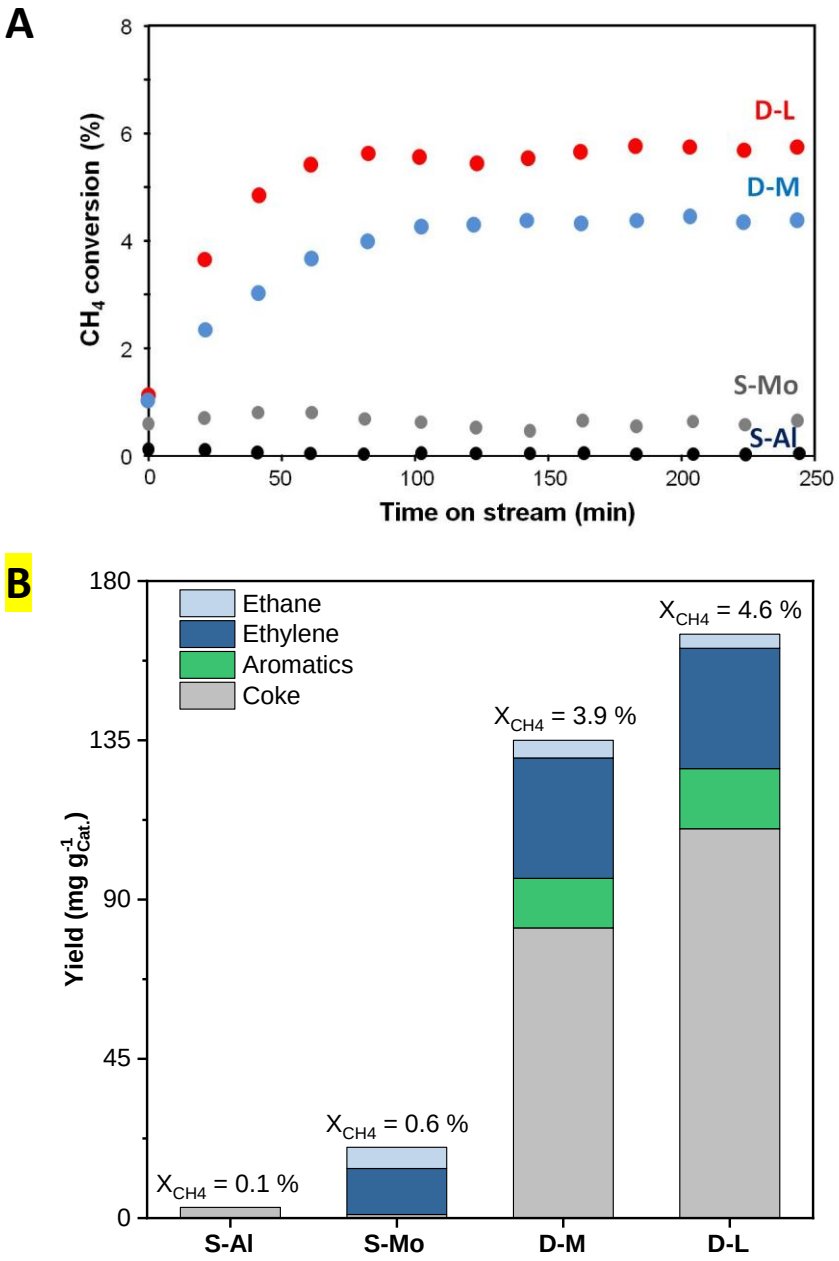

Figure 3. (A) CH_4 conversion as a function of time on stream on S-Mo, S-Al and dual (D-L and D-M) catalysts, (B) bar chart of yields of products and CH_4 conversion (milligrams per gram of catalyst, *i. e.* sum of yields, and %: above the bar charts), during the time on stream window of 0 – 250 min. Reaction conditions: T = 850 °C, P = 1 bar, WHSV = 1.2 h^{-1}.

3.2 Characterization of spent and regenerated catalysts.

The combustion of the carbonaceous deposits on the acidic (S-Al-L-AR) and metal (S-Mo-L-AR) catalysts is monitored by TG (Figure S1) and DTG, (Figure 4) [19]. Three types of coke were identified earlier on Mo/ZSM-5 catalysts prepared by wet impregnation [29]: (*i*) light

carbonaceous species associated with Mo-carbides, (*ii*) soft or amorphous coke located close to Mo carbide particles, (*iii*) hard or graphitic coke made of polyaromatic hydrocarbons (PAHs). S-Al-L-AR, S-Mo-L-AR and D-M-AR catalysts contain only hard coke, formed by condensation of aromatic molecules on BAS [29,30]. In the layered configuration (D-L), coke is located mostly on the acidic layer (S-Al-L-AR), while the upper layer (S-Mo-L-AR) is almost free of coke (Figure S1). In the D-M configuration, the dilution of the active coke-producing catalyst (S-Al) with the S-Mo leads to a coke content of D-M-AR between those of the two layers of the D-L configuration (Figure S1). Here as "coke" we considered not only the carbon deposited on the catalyst but also all the condensed hydrocarbons determined by the material balance. A catalyst consisting of Mo introduced in the framework of an acidic ZSM-5, [Mo]ZSM-5, reported previously by our group displays an homogeneous coke distribution on the particles [14].

Under MDA operating conditions, classical Mo zeolite catalysts deactivate by migration and sintering of molybdenum carbides weakly bound to the zeolite [31]. During the exothermic catalyst regeneration, molybdenum carbide is oxidized and steam generated by the coke combustion. Such conditions favor zeolite dealumination and the extra-framework aluminum generated react with mobile Mo species forming stable aluminum molybdates, leading to irreversible catalyst deactivation [29,32].

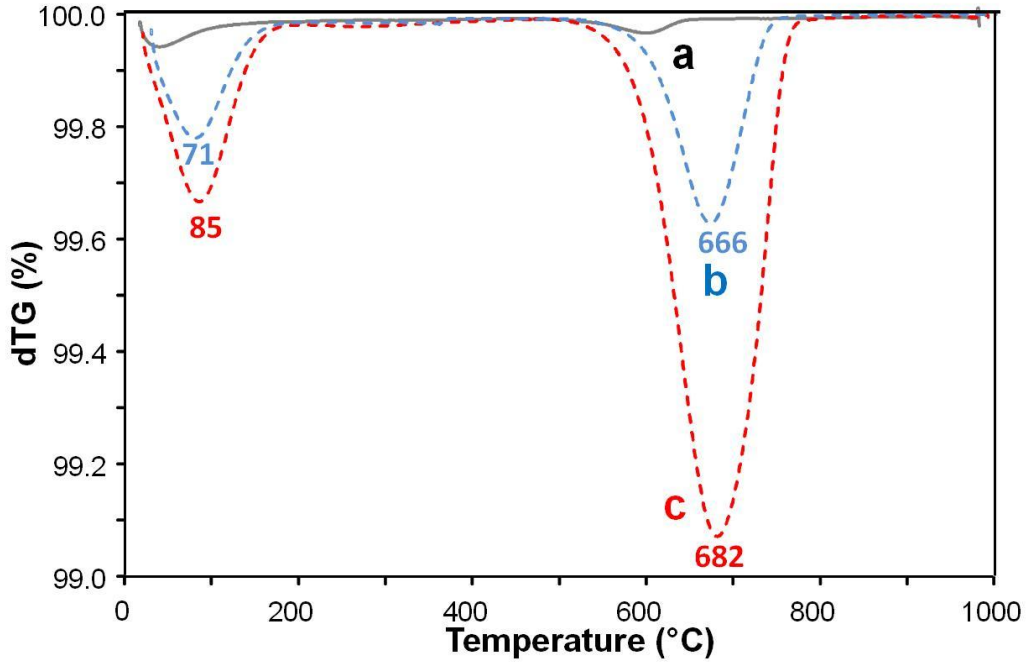

Figure 4. DTG monitoring of the temperature programmed combustion of coke on spent catalysts: (a) S-Mo-L-AR from the layered D-L-AR catalyst (black), (b) D-M-AR catalyst (blue)

and (c) S-Al-L-AR layer from D-L-AR (red). The low temperature peak corresponds to water desorption. Conditions: T: 25-1000 °C, ramp rate: 10 °/min, air flow rate: 40 ml/min.

TEM highlights the morphology and zeolite crystal size, before and after reaction (Figure S2). The S-Al crystal size is about 200 nm while the spherical S-Mo is around 100 nm. No amorphous phase is present, even in the spent catalysts indicating that crystallinity is maintained even after the severe conditions during reaction and regeneration.

The crystallinity of the S-Al catalyst before and after reaction followed by regeneration is monitored by XRD (Figure S3(A)). All Bragg peaks in the fresh and regenerated catalysts are present, indicating that the MFI structure is preserved. Le Bail refinement (Table 2) indicates that both S-Al and S-Al-L-AR-R unit cells are orthorhombic, and a unit cell volume decrease for S-Al-AR-R (Table 2) indicative of partial dealumination. The XRD patterns of S-Mo and S-Mo-L-AR-R, Figure S3(B-C), exhibit the characteristic splitting of the 23.30-23.4, 23.7-23.8 and 24.3-24.6 °2θ peaks (marked with an asterisk), indicative of a monoclinic symmetry (Table 2). This is in line with our previous work showing that insertion of Mo in the MFI framework triggers an orthorhombic to monoclinic transition [14,28]. The monoclinic symmetry for both S-Mo and S-Mo-L-AR-R indicates that Mo atoms originally present in the framework stay in the structure even after catalytic reaction at 850 °C and subsequent regeneration at 700 °C. The increased unit cell volume observed on zeolites containing Mo (S-Mo and S-Mo-L-AR-R) is also a strong indication of the presence of framework Mo and the high stability of such catalysts [33,34]. Le Bail refinement (Table 2) indicates a slight expansion in the unit cell volume of S-Mo-L-AR-R. This could be attributed to a more homogeneous spatial (re)distribution of Mo atoms in the crystals due to the high temperatures during the CH_4 conversion. The S-Mo catalyst displays excellent thermal and hydrothermal stabilities during reaction-regeneration, ensuring a stable operation of the derived layered catalyst (D-L) in successive catalytic cycles.

The homogeneity of the Si environment and high crystallinity of the S-Mo-L-AR-R catalyst is also illustrated by ^{29}Si NMR spectroscopy (Figure S4A). The high resolution of the Q^4 peaks after a reaction-regeneration cycle and the absence of a Q^3 peak confirm that this Al-free Mo-single-site zeolite catalyst is still almost devoid of silanol defects [28,35]. The absence of a Q^3 peak in the S-Mo-L-AR-R spectra indicates that during the reaction-regeneration cycle no Mo or Si leaves the zeolite structure for extra framework positions as such a move would result in

the creation of silanol nests. On the contrary, the ^{29}Si NMR spectra of the S-Al and S-Al-L-AR-R catalysts, Figure S4B, show less resolved Q^4 indicative of the presence of silanols. For the aluminum containing catalysts (S-Al and S-Al-L-AR-R), the Q^3 peak points to both the presence of extra-framework Al (EFAL) and silanol defects [28]. The intensity of the Q^3 peak decreases after the reaction-regeneration cycle indicative of a partial zeolite dealumination generating EFAL (octahedral) Al. This is confirmed by ^{27}Al NMR, Figure 5: the S-Al-L-AR-R spectra have a lower peak intensity at 55 ppm (tetrahedral Al) relative to the 0 ppm (octahedral Al), compared to S-Al. In a nutshell, during methane conversion and its subsequent regeneration, the monofunctional S-Mo, S-Mo-L-AR-R does not suffer from irreversible damage to its structure as no framework Mo is lost and no coke is deposited, ensuring reproducible performance during reaction/regeneration cycles.

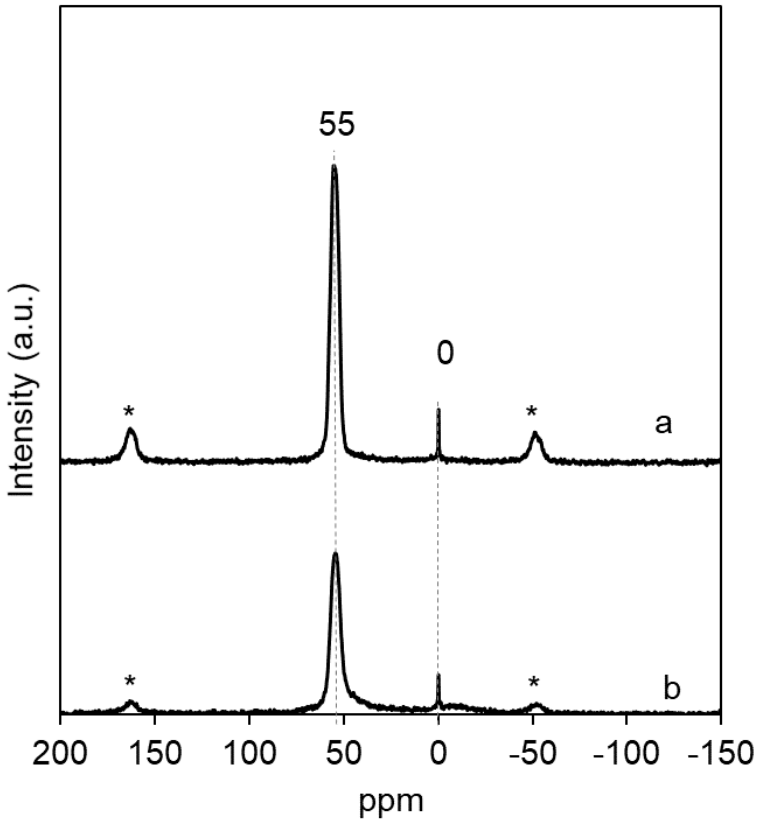

Figure 5. ^{27}Al MAS NMR spectra of the S-Al catalyst: (a) before reaction, (b) after methane conversion and regeneration at 700 °C (S-Al-L-AR-R). Asterisks mark the spinning side bands.

3.3 Stability of dual catalysts in reaction-regeneration cycles.

The time on stream stability of the two dual catalysts, D-M and D-L, after two cycles of reaction (*i.e.*, reducing conditions) and regeneration by coke combustion (*i.e.*, oxidative conditions) is reported in Figure 6 and aromatics yield is more typical for an MDA reaction [29]. After an initial increase, benzene yields drop after about 120 min (D-L) and 150 min (D-M) due to coke deactivation of its ZSM-5 zeolite (S-Al) component. At the same time, the C_2 yield increases and reaches a plateau, indicating that the Mo active sites in both configurations are preserved (Figure 6C).

The catalytic performances, conversion as well as aliphatic and aromatic yields, of a regenerated D-M catalyst are degraded due to the partial dealumination of the S-Al (H-ZSM-5) component. On the contrary, under identical conditions, the performance of the layer catalyst (D-L) after regeneration is preserved since a new S-Al component was added at the regeneration step. This indicates that as long as Mo remains in the zeolite framework of the S-Mo component of the dual catalyst, reproducible behavior is maintained under cycling conditions.

These results highlight an important and fundamental difference between these novel and the classical MDA catalysts where one cause of irreversible deactivation is the loss of the Mo activity as reported by Kosinov *et al.* [2]. Our novel D-L catalyst could therefore work in a stacked bed mode where the two components of the dual catalysts function at their optimal operating conditions (*e.g.* temperature, contact time) as applied, for instance, in hydroprocessing of oil fractions [36].

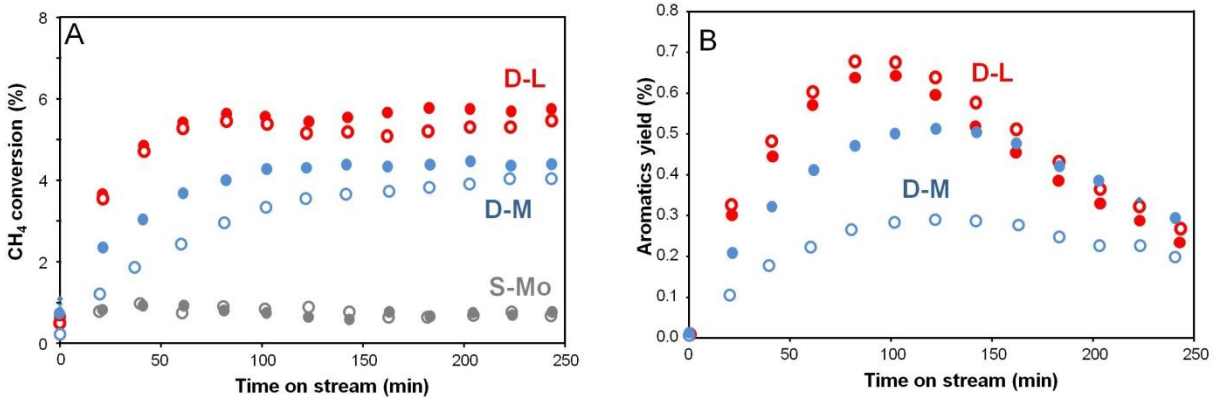

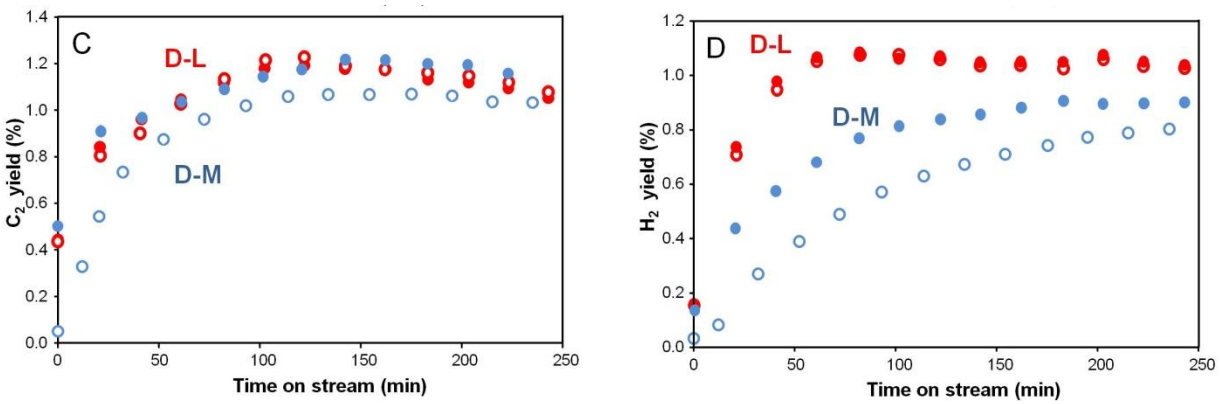

Figure 6. (A) CH_4 conversion as a function of time on stream for the single S-Mo catalyst, dual catalysts in layered (D-L) and mixed (D-M) configurations after a first (filled circles) run and a second (open circles) run separated by a regeneration, (B) C-based aromatics yield, (C) C-based aliphatics yield, and (D) hydrogen yield after the first and second consecutive cycles of reaction-regeneration as a function of time on stream of D-M and D-L catalysts. Reaction conditions: T = 850 °C, P = 1 bar, WHSV = 1.2 h^{-1}.

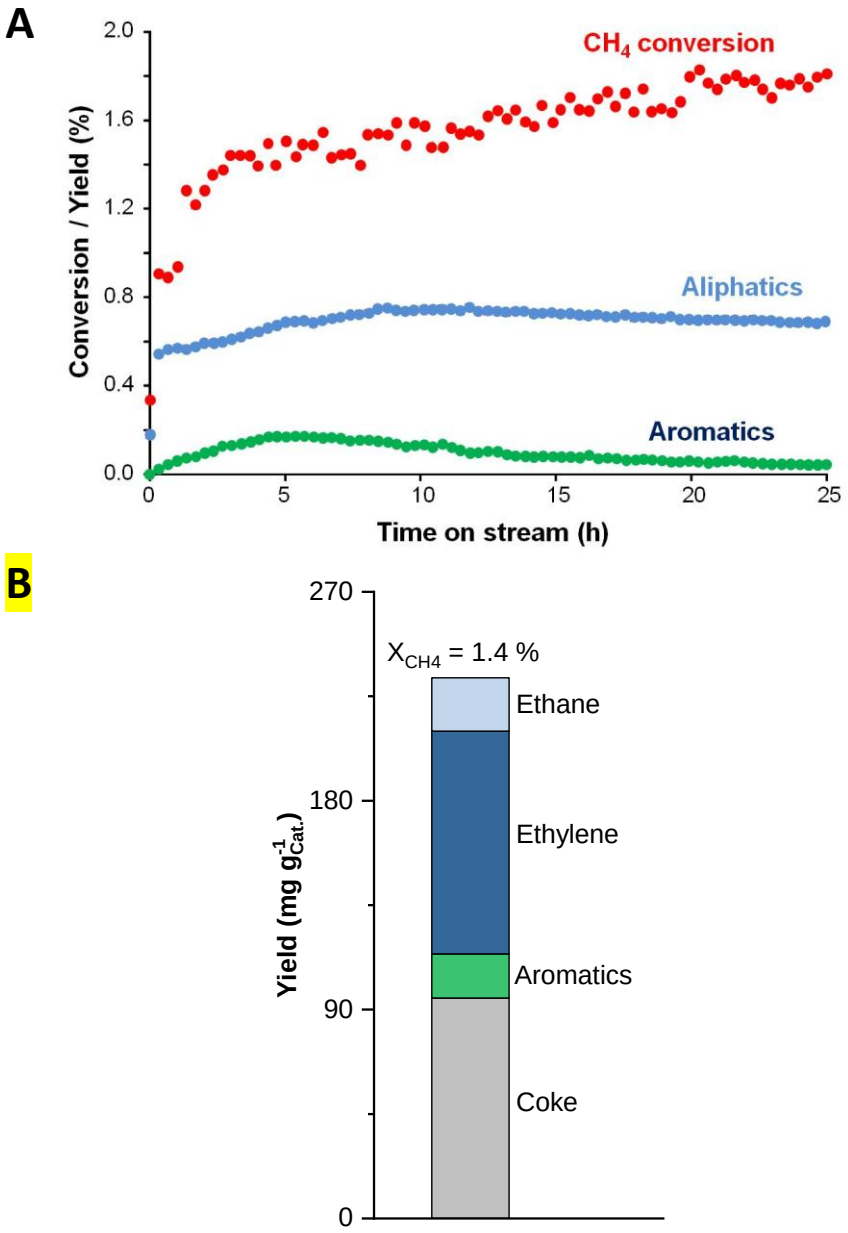

Figure 7 (A) CH_4 conversion, carbon-based yields of aromatics and aliphatics as a function of time on stream for the D-L catalyst with S-Mo (top) at 850 ºC and S-Al (bottom) at 450 ºC, (B) bar chart of yields of products and CH_4 conversion (milligrams per gram of catalyst, *i. e.* sum of yields, and %: above the bar charts), during the time on stream window of 0 – 20 h on the D-L catalyst. Reaction conditions: S-Mo layer at T = 850 °C, S-Al layer at 450 °C, P = 1 bar, WHSV = 1.2 h^{-1}.

As a main cause of catalyst deactivation is coke formation on the S-Al acidic catalyst at high reaction temperature (850 °C), a possible solution could be to decrease the temperature only for the S-Al catalyst. For this purpose, a S-Al layer is placed at the bottom of the reactor with the temperature set at 450 °C while the upper layer temperature, containing only S-Mo is 850 °C. While with a lower temperature in the S-Al zeolite layer of a D-L catalyst, methane conversion is lower than with a uniform temperature of 850 °C in both layers (Figure 7), the deactivation by coking is mitigated and a relatively stable production of aliphatics and aromatics last for at least 25 h.

In summary, we reported the transformation of methane using the formulation of two monofunctional catalysts occurring at high temperature (850 °C). The S-Mo catalyst did not suffer from structural damage and lost and/or agglomeration of Mo after cycling catalytic tests, while the deposition of coke in the S-Al acidic catalyst was observed. As “coke” we considered not only the carbon deposited on the catalyst but also all the heavy condensed hydrocarbons determined by the material balance. The coke was formed mainly on the S-Al acidic catalyst and the possible solution to decrease will be to reduce the reaction temperature only for that catalyst. Thus the CH_4 activation will take place at 850 °C using the stable S-Mo catalyst, while decreasing the temperature on the S-Al acidic catalyst will result in lower selectivity to "coke" (condensed hydrocarbons) without substantial change in the targeted product distribution on the acidic catalyst.

4. Conclusions

A monofunctional Mo-zeolite catalyst (S-Mo) displays superior thermal and hydrothermal (steaming during continuous reaction-regeneration cycles) stability in converting methane to hydrogen and higher hydrocarbons as atomically dispersed Mo is maintained in a zeolite framework devoid of silanol defects. Its catalytic performance can be significantly improved (methane conversion and hydrocarbon yield) by combining it with a monofunctional acidic zeolite (S-Al) catalyst operating at much lower and more optimal temperature.

The main reason for the deactivation of the dual catalysts is now coke deposition on the purely acidic zeolite, S-Al, and its partial dealumination during regeneration. On the other hand, the S-Mo catalyst produces negligible amounts of coke and keeps it structural integrity, *i.e.*, atomic dispersion of Mo in a zeolitic framework. The issue of deactivation of an acidic zeolite by coking and framework dealumination is well-known and already addressed in many processes (e.g., FCC) where:

- coked catalysts are promptly transferred to a regeneration zone where coke is burned and the CO_2 produced can be captured. The regenerated catalysts bring most of the heat of combustion to the endothermic reaction zone
- zeolite dealumination can be mitigated by embedding in a matrix [37] and treatment with phosphorous based additives [38–40].

The main benefit of a system based on two different monofunctional catalysts operating under optimized conditions is to avoid an irreversible deactivation of a bi-functional catalyst and replace it by a more manageable reversible deactivation as in already well-known and practiced processes.

While the irreversible catalyst deactivation challenge in methane to hydrogen and valuable hydrocarbons is on its way to being solved, other issues need further attention, namely catalytic activity and selectivity are still outstanding. Preliminary results [41] show that the level of Mo incorporation can be increased significantly while maintaining the high thermal and hydrothermal stabilities reported here. A commercially viable process to extract hydrogen from natural gas and capture its carbon and remaining hydrogen as added value chemicals (olefins and aromatics) is not yet around the corner but an important roadblock along this path is probably on its way to be removed.

Acknowledgements

This research was supported by TOTAL and the ANR-TOTAL Industrial Chair "NanoCleanEnergy" and the Normandy Region through the Lable of Excellence for the Centre of zeolites and nanoporous materials (CLEAR).

References

[1] R.Y. Chiao, M.L. Cohen, A.J. Leggett, W.D. Phillips, C.L.H. Jr, Visions of Discovery: New Light on Physics, Cosmology, and Consciousness, Cambridge University Press, 2011.
[2] N. Kosinov, F.J.A.G. Coumans, E.A. Uslamin, A.S.G. Wijpkema, B. Mezari, E.J.M. Hensen, Methane Dehydroaromatization by Mo/HZSM-5: Mono- or Bifunctional Catalysis?, ACS Catal. 7 (2017) 520–529. https://doi.org/10.1021/acscatal.6b02497.
[3] Z. Zakaria, S.K. Kamarudin, Direct conversion technologies of methane to methanol: An overview, Renew. Sustain. Energy Rev. 65 (2016) 250–261. https://doi.org/10.1016/j.rser.2016.05.082.
[4] S. Ma, X. Guo, L. Zhao, S. Scott, X. Bao, Recent progress in methane dehydroaromatization: From laboratory curiosities to promising technology, J. Energy Chem. 22 (2013) 1–20. https://doi.org/10.1016/S2095-4956(13)60001-7.

[5] M.C. Alvarez-Galvan, N. Mota, M. Ojeda, S. Rojas, R.M. Navarro, J.L.G. Fierro, Direct methane conversion routes to chemicals and fuels, Catal. Today. 171 (2011) 15–23. https://doi.org/10.1016/j.cattod.2011.02.028.
[6] A. Aseem, M.P. Harold, C2 yield enhancement during oxidative coupling of methane in a nonpermselective porous membrane reactor, Chem. Eng. Sci. 175 (2018) 199–207. https://doi.org/10.1016/j.ces.2017.09.035.
[7] Y. Chen, X. Wang, X. Luo, X. Lin, Y. Zhang, Non-Oxidative Methane Conversion Using Lead- and Iron-Modified Albite Catalysts in Fixed-Bed Reactor, Chin. J. Chem. 36 (2018) 531–537. https://doi.org/10.1002/cjoc.201700800.
[8] D.P. Serrano, J.A. Botas, R. Guil-Lopez, H2 production from methane pyrolysis over commercial carbon catalysts: Kinetic and deactivation study, Int. J. Hydrog. Energy. 34 (2009) 4488–4494. https://doi.org/10.1016/j.ijhydene.2008.07.079.
[9] X. Guo, G. Fang, G. Li, H. Ma, H. Fan, L. Yu, C. Ma, X. Wu, D. Deng, M. Wei, D. Tan, R. Si, S. Zhang, J. Li, L. Sun, Z. Tang, X. Pan, X. Bao, Direct, Nonoxidative Conversion of Methane to Ethylene, Aromatics, and Hydrogen, Science. 344 (2014) 616–619. https://doi.org/10.1126/science.1253150.
[10] M. Młotek, J. Sentek, K. Krawczyk, K. Schmidt-Szałowski, The hybrid plasma–catalytic process for non-oxidative methane coupling to ethylene and ethane, Appl. Catal. Gen. 366 (2009) 232–241. https://doi.org/10.1016/j.apcata.2009.06.043.
[11] K. Sun, D.M. Ginosar, T. He, Y. Zhang, M. Fan, R. Chen, Progress in Nonoxidative Dehydroaromatization of Methane in the Last 6 Years, Ind. Eng. Chem. Res. 57 (2018) 1768–1789. https://doi.org/10.1021/acs.iecr.7b04707.
[12] Y. Xiang, H. Wang, J. Cheng, J. Matsubu, Progress and prospects in catalytic ethane aromatization, Catal. Sci. Technol. 8 (2018) 1500–1516. https://doi.org/10.1039/C7CY01878A.
[13] C. Karakaya, R.J. Kee, Progress in the direct catalytic conversion of methane to fuels and chemicals, Prog. Energy Combust. Sci. 55 (2016) 60–97. https://doi.org/10.1016/j.pecs.2016.04.003.
[14] S.V. Konnov, F. Dubray, E.B. Clatworthy, C. Kouvatas, J.-P. Gilson, J.-P. Dath, D. Minoux, C. Aquino, V. Valtchev, S. Moldovan, S. Koneti, N. Nesterenko, S. Mintova, Novel Strategy for the Synthesis of Ultra-Stable Single-Site Mo-ZSM-5 Zeolite Nanocrystals, Angew. Chem. Int. Ed. 59 (2020) 19553–19560. https://doi.org/10.1002/anie.202006524.
[15] M.T. Portilla, F.J. Llopis, C. Martínez, Non-oxidative dehydroaromatization of methane: an effective reaction–regeneration cyclic operation for catalyst life extension, Catal. Sci. Technol. 5 (2015) 3806–3821. https://doi.org/10.1039/C5CY00356C.
[16] Y. Yao, Z. Huang, P. Xie, L. Wu, L. Ma, T. Li, Z. Pang, M. Jiao, Z. Liang, J. Gao, Y. He, D.J. Kline, M.R. Zachariah, C. Wang, J. Lu, T. Wu, T. Li, C. Wang, R. Shahbazian-Yassar, L. Hu, High temperature shockwave stabilized single atoms, Nat. Nanotechnol. 14 (2019) 851–857. https://doi.org/10.1038/s41565-019-0518-7.
[17] P. Xie, T. Pu, A. Nie, S. Hwang, S.C. Purdy, W. Yu, D. Su, J.T. Miller, C. Wang, Nanoceria-Supported Single-Atom Platinum Catalysts for Direct Methane Conversion, ACS Catal. 8 (2018) 4044–4048. https://doi.org/10.1021/acscatal.8b00004.
[18] Y. Zeng, A. Kimura, P. Zhang, J. Liang, J. Fan, L. Xiao, C. Wang, G. Yang, X. Peng, N. Tsubaki, Resistance against Carbon Deposition via Controlling Spatial Distance of

Catalytic Components in Methane Dehydroaromatization, Catalysts. 11 (2021) 148. https://doi.org/10.3390/catal11020148.
[19] S. Liu, L. Wang, R. Ohnishi, M. Ichikawa, Bifunctional Catalysis of Mo/HZSM-5 in the Dehydroaromatization of Methane to Benzene and Naphthalene XAFS/TG/DTA/MASS/FTIR Characterization and Supporting Effects, J. Catal. 181 (1999) 175–188. https://doi.org/10.1006/jcat.1998.2310.
[20] F. Solymosi, J. Cserényi, A. Szöke, T. Bánsági, A. Oszkó, Aromatization of Methane over Supported and Unsupported Mo-Based Catalysts, J. Catal. 165 (1997) 150–161. https://doi.org/10.1006/jcat.1997.1478.
[21] S.-T. Tsai, P.-H. Chao, I. Wang, T.-C. Tsai, Dual-bed catalyst system for improving product purity and catalytic stability in alkylbenzene transalkylation, Appl. Catal. Gen. 385 (2010) 73–79. https://doi.org/10.1016/j.apcata.2010.06.047.
[22] N.A.S. Amin, S. Ammasi, Dual-Bed Catalytic System for Direct Conversion of Methane to Liquid Hydrocarbons, J. Nat. Gas Chem. 15 (2006) 191–202. https://doi.org/10.1016/S1003-9953(06)60026-1.
[23] B. Zohour, D. Noon, S. Senkan, Spatial Concentration and Temperature Profiles in Dual-Packed-Bed Catalytic Reactors: Oxidative Coupling of Methane, ChemCatChem. 6 (2014) 2815–2820. https://doi.org/10.1002/cctc.201402404.
[24] T.F. Degnan, Recent progress in the development of zeolitic catalysts for the petroleum refining and petrochemical manufacturing industries, in: R. Xu, Z. Gao, J. Chen, W. Yan (Eds.), Stud. Surf. Sci. Catal., Elsevier, 2007: pp. 54–65. https://doi.org/10.1016/S0167-2991(07)80825-1.
[25] C. Dittrich, A process for carrying out endothermic, heterogeneously catalyzed reactions, WO2015082375A1, 2015.
[26] V. Petříček, M. Dušek, L. Palatinus, Crystallographic Computing System JANA2006: General features, Z. Für Krist. - Cryst. Mater. 229 (2014) 345–352. https://doi.org/10.1515/zkri-2014-1737.
[27] T.I. Korányi, K. Föttinger, H. Vinek, J.B. Nagy, Characterization of aluminium siting in MOR and BEA zeolites by 27Al, 29Si NMR and FTIR spectroscopy, in: J. Čejka, N. Žilková, P. Nachtigall (Eds.), Stud. Surf. Sci. Catal., Elsevier, 2005: pp. 765–772. https://doi.org/10.1016/S0167-2991(05)80411-2.
[28] F. Dubray, S. Moldovan, C. Kouvatas, J. Grand, C. Aquino, N. Barrier, J.-P. Gilson, N. Nesterenko, D. Minoux, S. Mintova, Direct Evidence for Single Molybdenum Atoms Incorporated in the Framework of MFI Zeolite Nanocrystals, J. Am. Chem. Soc. 141 (2019) 8689–8693. https://doi.org/10.1021/jacs.9b02589.
[29] C.H.L. Tempelman, E.J.M. Hensen, On the deactivation of Mo/HZSM-5 in the methane dehydroaromatization reaction, Appl. Catal. B Environ. 176–177 (2015) 731–739. https://doi.org/10.1016/j.apcatb.2015.04.052.
[30] C.H.L. Tempelman, V.O. de Rodrigues, E.R.H. van Eck, P.C.M.M. Magusin, E.J.M. Hensen, Desilication and silylation of Mo/HZSM-5 for methane dehydroaromatization, Microporous Mesoporous Mater. 203 (2015) 259–273. https://doi.org/10.1016/j.micromeso.2014.10.020.
[31] P. Schwach, X. Pan, X. Bao, Direct Conversion of Methane to Value-Added Chemicals over Heterogeneous Catalysts: Challenges and Prospects, Chem. Rev. 117 (2017) 8497–8520. https://doi.org/10.1021/acs.chemrev.6b00715.

[32] B.S. Liu, J.W.H. Leung, L. Li, C.T. Au, A.S.-C. Cheung, TOF-MS investigation on methane aromatization over 3%Mo/HZSM-5 catalyst under supersonic jet expansion condition, Chem. Phys. Lett. 430 (2006) 210–214. https://doi.org/10.1016/j.cplett.2006.08.131.
[33] A. Tuel, Y.B. Taaˆrit, Influence of the nature of silicon and titanium alkoxides on the incorporation of titanium in TS-1, Appl. Catal. Gen. 110 (1994) 137–151. https://doi.org/10.1016/0926-860X(94)80112-6.
[34] R.Ch. Deka, V.A. Nasluzov, E.A. Ivanova Shor, A.M. Shor, G.N. Vayssilov, N. Rösch, Comparison of All Sites for Ti Substitution in Zeolite TS-1 by an Accurate Embedded-Cluster Method, J. Phys. Chem. B. 109 (2005) 24304–24310. https://doi.org/10.1021/jp050056l.
[35] J.M. Chezeau, L. Delmotte, J.L. Guth, Z. Gabelica, Influence of synthesis conditions and postsynthesis treatments on the nature and quantity of structural defects in highly siliceous MFI zeolites: A high-resolution solid-state 29Si n.m.r. study, Zeolites. 11 (1991) 598–606. https://doi.org/10.1016/S0144-2449(05)80011-9.
[36] J. Ancheyta, A. Alvarez-Majmutov, C. Leyva, Hydrotreating of oil fractions, in: Multiph. Catal. React., John Wiley & Sons, Ltd, 2016: pp. 295–329. https://doi.org/10.1002/9781119248491.ch13.
[37] Z.M.M. Noronha, J.L.F. Monteiro, P. Gélin, The role of matrix embedding on the properties of steamed mordenites, Microporous Mesoporous Mater. 23 (1998) 331–344. https://doi.org/10.1016/S1387-1811(98)00135-8.
[38] T. Blasco, A. Corma, J. Martínez-Triguero, Hydrothermal stabilization of ZSM-5 catalytic-cracking additives by phosphorus addition, J. Catal. 237 (2006) 267–277. https://doi.org/10.1016/j.jcat.2005.11.011.
[39] H.E. van der Bij, F. Meirer, S. Kalirai, J. Wang, B.M. Weckhuysen, Hexane Cracking over Steamed Phosphated Zeolite H-ZSM-5: Promotional Effect on Catalyst Performance and Stability, Chem. – Eur. J. 20 (2014) 16922–16932. https://doi.org/10.1002/chem.201404924.
[40] T.F. Degnan, G.K. Chitnis, P.H. Schipper, History of ZSM-5 fluid catalytic cracking additive development at Mobil, Microporous Mesoporous Mater. 35–36 (2000) 245–252. https://doi.org/10.1016/S1387-1811(99)00225-5.
[41] I. Medeiros Costa, E. Dib, F. Dubray, J.-P. Gilson, J.-P. Dath, N. Nesterenko, H. Aleksandrov, G. Vayssilov, S. Mintova, Unraveling the effect of silanol defects on the insertion of single site Mo in the MFI zeolite framework, Inorg. Chem., Accepted for publication on December 20, 2021.